LETTER

doi:10.1038/nature25136

A large oxygen-dominated core from the seismic cartography of a pulsating white dwarf

N. Giammichele[1,2], S. Charpinet[1], G. Fontaine[2], P. Brassard[2], E. M. Green[3], V. Van Grootel[4], P. Bergeron[2], W. Zong[1,5] & M.-A. Dupret[4]

White-dwarf stars are the end product of stellar evolution for most stars in the Universe[1]. Their interiors bear the imprint of fundamental mechanisms that occur during stellar evolution[2,3]. Moreover, they are important chronometers for dating galactic stellar populations, and their mergers with other white dwarfs now appear to be responsible for producing the type Ia supernovae that are used as standard cosmological candles[4]. However, the internal structure of white-dwarf stars—in particular their oxygen content and the stratification of their cores—is still poorly known, because of remaining uncertainties in the physics involved in stellar modelling codes[5,6]. Here we report a measurement of the radial chemical stratification (of oxygen, carbon and helium) in the hydrogen-deficient white-dwarf star KIC08626021 (J192904.6+444708), independently of stellar-evolution calculations. We use archival data[7,8] coupled with asteroseismic sounding techniques[9,10] to determine the internal constitution of this star. We find that the oxygen content and extent of its core exceed the predictions of existing models of stellar evolution. The central homogeneous core has a mass of 0.45 solar masses, and is composed of about 86 per cent oxygen by mass. These values are respectively 40 per cent and 15 per cent greater than those expected from typical white-dwarf models. These findings challenge present theories of stellar evolution and their constitutive physics, and open up an avenue for calibrating white-dwarf cosmochronology[11].

Hydrogen-deficient DB-type white dwarfs are dying stars that have effective temperatures ranging from about 12,000 K to upwards of 35,000 K (ref. 12). They have undergone a late final flash as post-asymptotic-giant-branch (post-AGB) stars, which freed them from their thin remaining hydrogen envelope[13–15]. Their deeper chemical stratification—as in any typical white dwarf—is otherwise determined by the rate of the nuclear reaction $^{12}C(\alpha,\gamma)^{16}O$, which synthesizes oxygen from the ashes of the core-helium-burning phase, by means of mixing processes associated with convection and rotation as well as the number of thermal pulses that occur in evolved AGB stars[16]. The descendant DB white dwarfs must bear the signature of such processes in their core, as well as the imprint of the still-ongoing settling of carbon and oxygen in the surrounding helium-rich envelope.

KIC08626021 (GALEX J192904.6+444708) is the first pulsating DB white dwarf (also known as the V777 Her class of variable stars) to be monitored extensively by the Kepler spacecraft for its pulsation properties[8]. This star shows an oscillation spectrum composed of non-radial g-modes, which are potentially sensitive to the deep interior of the star[17]. Using an analysis of 23 months of Kepler high-precision photometric data[18], we exploit the eight well secured independent modes, which have periods ranging from 143.2 s to 376.1 s (Fig. 1, Extended Data Table 1 and Methods). These relatively short pulsation periods are—according to the period–luminosity relation[17]—typical of the blue (hot) edge of the V777 Her instability strip, as confirmed by our spectroscopic determination of the atmospheric parameters $T_{\rm eff}$ (effective temperature; 29,360 ± 780 K) and $\log(g)$ (7.89 ± 0.05) (see Methods and Extended Data Fig. 1).

The seismic analysis performed here relies on a forward-modelling technique using parameterized static stellar models, which is independent of stellar-evolution calculations. This independence is crucial for providing an objective determination of the chemical stratification in the core of white-dwarf stars. Our analysis differs fundamentally from several previous attempts to provide asteroseismic constraints on such stars that rely on evolutionary models[19] and therefore carry with them the many uncertainties of such models. Here, we take advantage of our most recent developments in the definition of parameterized white-dwarf models for asteroseismology[9,10]. This method allows a flexible and exhaustive exploration of the structural configuration (core and envelope) of white dwarfs that outperforms all comparable approaches that have been attempted in the past. A historical and critical review of all of these developments has been presented recently[9]. In particular, none of these attempts has succeeded in reproducing accurately the observed periods and in securely extracting an independent measure of the core stratification. In a nutshell (see Methods for more details and Extended Data Fig. 2), we use a shape-optimization technique based on Akima splines to produce smooth, adjustable oxygen profiles in the core. This profile is optimized simultaneously with other parameters that define the star's full hydrostatic structure and the chemical stratification in its envelope. With this technique, we can ultimately recover, along with global parameters, the optimal model chemical stratification for the main constituents (here carbon, oxygen and helium) that is best able to reproduce the seismic observables, as hare-and-hounds experiments have demonstrated[10].

When applied to KIC08626021, the seismic solution is uniquely determined around a well defined minimum of the fitted merit function in parameter space (see Methods, Extended Data Figs 3 and 4, and Extended Data Table 2). The optimal model is found to have $T_{\rm eff} = 29{,}968 \pm 200$ K and $\log(g) = 7.917 \pm 0.009$, which match perfectly the independent measurements obtained from spectroscopy (within 0.8σ for the effective temperature and 0.5σ for the surface gravity). Other seismic inferences are provided in Table 1. The seismic values given in that table are derived from the optimal model solution, and the associated errors represent internal errors of the fit corrected with an estimation of external errors due to known potential systematics. These errors are evaluated from the likelihood function covering the full parameter space that is sampled during the optimization procedure[20] (Methods).

We find that the seismic fit perfectly reproduces the measured frequencies—that is, the seismic fit is well within the precision of the observations estimated at $\Delta\nu = 0.6$ nHz (or equivalently at $\Delta P = 38$ μs for the period measurements) for this dataset (Extended Data Table 1). Note that, with nearly two years of Kepler data, the precision of the

[1]Institut de Recherche en Astrophysique et Planétologie (IRAP), Université de Toulouse, Centre National de la Recherche Scientifique (CNRS), UPS, Centre National d'Études Spatiales (CNES), 14 Avenue Edouard Belin, F-31400 Toulouse, France. [2]Département de Physique, Université de Montréal, Montréal, Québec H3C 3J7, Canada. [3]Steward Observatory, University of Arizona, 933 North Cherry Avenue, Tucson, Arizona 85721, USA. [4]Space sciences, Technologies and Astrophysics Research (STAR) Institute, Université de Liège, 19C Allée du six-août, B-4000 Liège, Belgium. [5]Department of Astronomy, Beijing Normal University, Beijing 100875, China.

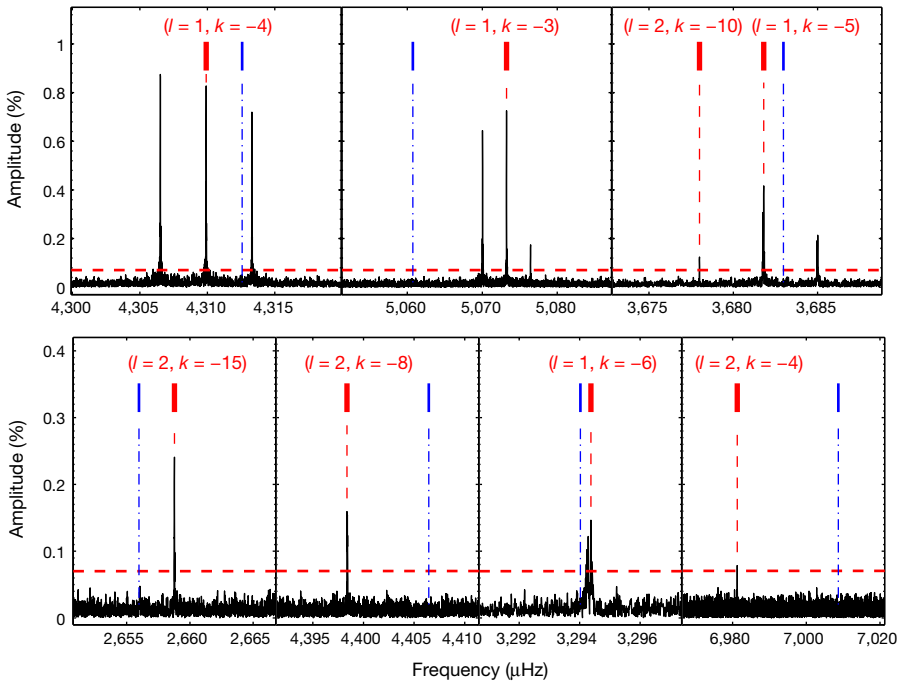

Figure 1 | Segments of the Lomb–Scargle periodogram for KIC08626021. This periodogram shows the pulsation amplitude (as a percentage) of the star's mean brightness versus frequency around detected signals (in μHz), superimposed with the matched theoretical frequencies obtained from our optimal seismic model (red; eight gravity modes) and the latest published results for this star[21] (blue; seven modes). Our asteroseismic modelling solution is able to reproduce the eight main observed pulsation periods in KIC08626021 at the precision of the observations (see Extended Data Table 1). That solution provides the mode identification shown here in terms of the degree index l and radial order k. The other statistically significant peaks are part of frequency multiplets best explained in terms of rotational splitting (see Methods and Extended Data Fig. 6).

measured frequencies is extremely high. Consequently, this new seismic solution outperforms, by orders of magnitude, any former analysis, including the most recent result obtained for the same star, which could match the frequencies only to an average precision of $\Delta\nu = 7.8\,\mu$Hz (ref. 21; see Fig. 1). This major improvement in the global precision of the fit allows for a precise derivation of the internal stratification. The distribution of the oxygen mass fraction in the core of the star—which has remained mostly unconstrained thus far—can now be unambiguously derived, along with profiles for the other main chemical species (Fig. 2 and Extended Data Fig. 5).

We find that the central abundance of oxygen rises up to 86.2% (±4%), that is, 15% more than is predicted from evolutionary calculations[2]. The extent of the homogeneous central part of the core is nearly doubled, reaching a fractional mass depth of $\log(q) \approx -0.7$ (or 0.45 solar masses, $M_\odot$), instead of $\log(q) \approx -0.35$ ($0.32M_\odot$). According to standard evolutionary calculations, this homogeneous region derives from the former convective, helium-burning core, which is possibly enlarged by a non-negligible region (up to 25% in mass) that is composed of the ashes of a rather thick, helium-burning shell across a predicted partially mixed zone (the former semi-convective layers), and is ultimately fully homogenized owing to Rayleigh–Taylor instabilities[22]. Recently, however, models that match the average spacing of pulsation periods observed in core-helium-burning red-clump stars have favoured a treatment of the core boundary that is enlarged by substantial overshoot (the so-called maximal overshoot model); these models do not produce a partial mixing zone (there is no semi-convection)[23]. In that situation, the oxygen plateau in the white-dwarf core may entirely be associated with the final extent of the fully mixed helium-burning core. This suggests that the extent of the progenitor convective core during the core-helium-burning phase should have encompassed masses of between $0.34M_\odot$ and $0.45M_\odot$—larger by a factor of between 1.1 (in the case of the maximal semi-convection zone predicted) and 1.4 (in the absence of a semi-convection zone). Interestingly, similar trends involving a large convective

Table 1 | Derived properties of KIC08626021

Quantity	Estimated value
$\log[g\ (\mathrm{cm\ s^{-2}})]$	7.92 ± 0.01
T_{eff} (K)	29,968 ± 198
$X(\mathrm{He})_{\mathrm{env}}$	0.18 ± 0.04
$\log(q_1)$	−7.63 ± 0.2
$\log(q_2)$	−3.23 ± 0.1
$X(\mathrm{O})_{\mathrm{centre}}$	0.86 ± 0.04
$\log(q_3)$	−0.72 ± 0.03
$M(\mathrm{He})/M_*$	0.0113% ± 0.006%
$M(\mathrm{C})/M_*$	21.96% ± 4.2%
$M(\mathrm{O})/M_*$	78.03% ± 4.2%
$M_*/M_\odot$	0.570 ± 0.005
$R_*/R_\odot$	0.0138 ± 0.0001
$L_*/L_\odot$	0.137 ± 0.005
M_{r}^*	10.28 ± 0.03
d (pc)†	422 ± 45
P_{rot} (h)	46.3 ± 2.5
V_{eq} (km s^{-1})	0.36 ± 0.02
J (kg m^2 s^{-1})‡	$(6.59 \pm 0.38) \times 10^{38}$
$J/J_\odot$	1/291
$\mathrm{d}P/\mathrm{d}t_{197}$ (s s^{-1})¶	14.4×10^{-14} or 2.8×10^{-14}
$\mathrm{d}P/\mathrm{d}t_{232}$ (s s^{-1})¶	15.1×10^{-14} or 2.8×10^{-14}
$\mathrm{d}P/\mathrm{d}t_{271}$ (s s^{-1})¶	15.5×10^{-14} or 3.0×10^{-14}
t_{cool} (yr)	$(8.43 \pm 0.05) \times 10^6$

Along with primary quantities coming directly from our seismic analysis, several secondary properties are also derived as explained in Methods. X(He), mass fraction of helium; $\log(q_1)$, the fractional mass depth where the local value of the He mass fraction equals $(1 + X(\mathrm{He})_{\mathrm{env}})/2$ (where $X(\mathrm{He})_{\mathrm{env}}$ is the mass fraction of He in the mixed zone of the star's envelope); $\log(q_2)$, the depth at which that mass fraction equals $X(\mathrm{He})_{\mathrm{env}}/2$; M(He), M(C) and M(O), mass of helium, carbon and oxygen, respectively; M_*, R_* and L_*, mass, radius and luminosity of the star, correspondingly; M_{r}, absolute magnitude in the r-band; d, distance to Earth (in parsecs); P_{rot}, rotation period; V_{eq}, equatorial velocity; J, total angular momentum; $\mathrm{d}P/\mathrm{d}t_x$, rate of period change of the mode with period x (in units of seconds per second), with (first number) or without (second number) neutrino emission; t_{cool}, cooling time of the star.
*Based on a model atmosphere with the seismic values of $\log(g)$, T_{eff} and M_*, coupled to the uncertain value of the Sloan Digital Sky Survey magnitude $r = 18.40 \pm 0.20$ for KIC08626021.
†Assuming no reddening.
‡Assuming solid-body rotation throughout the star.
¶With and without neutrino cooling.

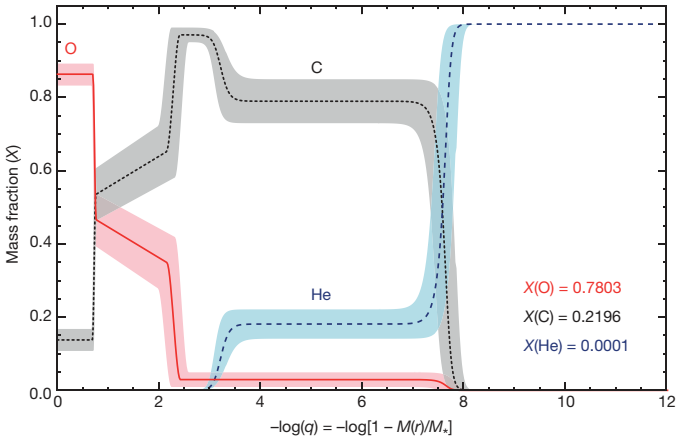

Figure 2 | Derived chemical stratification. The graph shows the distribution of oxygen (in red), carbon (in grey) and helium (in blue) obtained from the optimal seismic model. The estimated 1σ errors (shaded areas around each curve) are derived from the probability distributions calculated during the optimization process (Methods).The x axis shows the fractional mass depth (with $\log(q) = 0$ corresponding to the centre of the star). The total mass fractions for each element are indicated at the bottom right.

core were disclosed in a study of pulsating hot B subdwarf (sdB) stars[24–26], in particular because in these cases the probed cores may not yet have reached their maximal extent. These results will allow researchers to exclude mixing schemes that cannot produce enough oxygen or extended cores, and guide a better understanding of mixing processes.

The behaviour of the two outward descents in the oxygen mass stratification that bear the imprint of helium-shell-burning processes from earlier stages of evolution does not differ notably from the predictions of standard evolutionary calculations. The total oxygen content of the white-dwarf core reaches 78.0%±4.2%, much higher than the expected value of around 64% for a standard evolutionary white-dwarf model of the same mass[2]. Remarkably, we note the absence in our solution of a triple transition in which carbon, oxygen and helium coexist—a feature usually expected from evolution calculations. Although puzzling at first sight, this issue could be explored in relation to the number of thermal pulses that occur to erode the bottom of the helium envelope during post-AGB evolution[3], particularly given that KIC08626021's envelope is found to be quite thin. Finally, our finding of a double-layered helium envelope fits with the presently accepted scenario involving ongoing settling of helium after the late thermal pulse that produced this DB white dwarf. Overall, these new seismic constraints offer opportunities for testing stellar-evolution models and their constitutive physics (particularly processes that include convection, overshooting, semi-convection, and nuclear physics). The next step will be to explore late stages of stellar evolution, with the goal of reproducing the seismically derived chemical stratification of the white-dwarf core.

The chemical profile derived here from asteroseismology, applied to computations of white-dwarf cooling ages, leads to an estimate of $(8.43 \pm 0.05) \times 10^6$ yr for the cooling age of KIC08626021, independently of its pre-white-dwarf history. By comparison, uncertainties in the rates of nuclear reactions in the pre-white-dwarf phases alone lead to an uncertainty on that age that is ten times larger[5] than the uncertainty calculated above. Hence, the asteroseismological approach described here provides a powerful calibration of the internal composition profile of white dwarfs, with direct benefit to cosmochronology.

Finally, the total carbon/oxygen ratio found here for KIC08626021—which is lower than expected—has implications for studies of type Ia supernovae[27]. A smaller carbon/oxygen ratio leads to less ^{56}Ni being produced during the supernova explosion. This has a direct impact on the light curve of a type Ia supernova (which is powered by the decay of ^{56}Ni), with repercussions for cosmology, where these supernovae are widely used as standard candles and probes—notably for determining the cosmological equation of state.

Online Content Methods, along with any additional Extended Data display items and Source Data, are available in the online version of the paper; references unique to these sections appear only in the online paper.

Received 9 June; accepted 7 November 2017.
Published online 8 January 2018.

1. Fontaine, G. & Wesemael, F. in *Encyclopedia of Astronomy and Astrophysics 1894–1901 (IOP, 2000).*
2. Salaris, M., Cassisi, S., Pietrinferni, A., Kowalski, P. M. & Isern, J. A large stellar evolution database for population synthesis studies. VI. White dwarf cooling sequences. *Astrophys. J.* **716,** 1241–1251 (2010).
3. De Gerónimo, F. C., Althaus, L. G., Córsico, A. H., Romero, A. D. & Kepler, S. O. Asteroseismology of ZZ Ceti stars with fully evolutionary white dwarf models. I. The impact of the uncertainties from prior evolution on the period spectrum. *Astron. Astrophys.* **599,** A21–A28 (2017).
4. Fontaine, G., Brassard, P. & Bergeron, P. The potential of white dwarf cosmochronology. *Publ. Astron. Soc. Pac.* **113,** 409–435 (2001).
5. Fields, C. E., Farmer, R., Petermann, I., Illiadis, C. & Timmes, F. X. Properties of carbon-oxygen white dwarfs from Monte Carlo stellar models. *Astrophys. J.* **823,** 46 (2016).
6. Salaris, M. White dwarf cosmochronology: techniques and uncertainties. *Proc. Int. Astron. Soc.* **258,** 287–298 (2009).
7. Gilliland, R. L. *et al.* Kepler asteroseismology program: introduction and first results. *Publ. Astron. Soc. Pac.* **122,** 131–143 (2010).
8. Østensen, R. H. *et al.* At last—a V777 Her pulsator in the Kepler field. *Astrophys. J.* **736,** L39–L44 (2011).
9. Giammichele, N., Charpinet, S., Fontaine, G. & Brassard, P. Toward high-precision seismic studies of white dwarf stars: parametrization of the core and tests of accuracy. *Astrophys. J.* **834,** 136–162 (2017).
10. Giammichele, N., Charpinet, S., Brassard, P. & Fontaine, G. The potential of asteroseismology for probing the core chemical stratification in white dwarf stars. *Astron. Astrophys.* **598,** A109–A116 (2017).
11. Tremblay, P.-E., Kalirai, J. S., Soderblom, D. R., Cignoni, M. & Cummings, J. White dwarf cosmochronology in the solar neighborhood. *Astrophys. J.* **791,** 92–100 (2014).
12. Berg eron, P. *et al.* A comprehensive spectroscopic analysis of DB white dwarfs. *Astrophys. J.* **737,** 28–51 (2011).
13. Iben, I., Jr, Kaler, J. B., Truran, J. W. & Renzini, A. On the evolution of those nuclei of planetary nebulae that experience a final helium shell flash. *Astrophys. J.* **264,** 605–612 (1983).
14. Herwig, F., Blöcker, T., Langer, N. & Driebe, T. On the formation of hydrogen-deficient post-AGB stars. *Astron. Astrophys.* **349,** L5–L8 (1999).
15. Miller Bertolami, M. M., Althaus, L. G., Serenelli, A. M. & Panei, J. A. New evolutionary calculations for the born again scenario. *Astron. Astrophys.* **449,** 313–326 (2006).
16. Straniero, O., Domìnguez, I., Imbriani, G. & Piersanti, L. The chemical composition of white dwarfs as a test of convective efficiency during core helium burning. *Astrophys. J.* **583,** 878–884 (2003).
17. Fontaine, G. & Brassard, P. The pulsating white dwarf stars. *Publ. Astron. Soc. Pac.* **120,** 1043–1096 (2008).
18. Zong, W., Charpinet, S., Vauclair, G., Giammichele, N. & Van Grootel, V. Amplitude and frequency variations of oscillation modes in the pulsating DB white dwarf star KIC08626021. The likely signature of nonlinear resonant mode coupling. *Astron. Astrophys.* **585** (A22), 1–14 (2016).
19. Romero, A.D. *et al.* Toward ensemble asteroseismology of ZZ Ceti stars with fully evolutionary models. *Mon. Not. R. Astron. Soc.* **420,** 1462–1480 (2012).
20. Giammichele, N., Fontaine, G., Brassard, P. & Charpinet, S. A new analysis of the two classical ZZ Ceti white dwarfs GD 165 and Ross 548. II. Seismic modeling. *Astrophys. J. Suppl. Ser.* **223,** 10–36 (2016).
21. Bischoff-Kim, A., Østensen, R. H., Hermes, J. J. & Provencal, J. Seven-period asteroseismic fit of the Kepler DBV. *Astrophys. J.* **794,** 39–46 (2014).
22. Salaris, M. *et al.* The cooling of CO white dwarfs: influence of the internal chemical distribution. *Astrophys. J.* **486,** 413–419 (1997).
23. Constantino, T., Campbell, S. W., Christensen-Dalsgaard, J., Lattanzio, C. & Stello, D. The treatment of mixing in core helium burning models—I. Implications for asteroseismology. *Mon. Not. R. Astron. Soc.* **452,** 123–145 (2015).
24. Van Grootel, V. *et al.* Early asteroseismic results from *Kepler*: structural and core parameters of the hot B subdwarf KPD 1943+4058 as inferred from *g*-mode oscillations. *Astrophys. J.* **718,** L97–L101 (2010).
25. Van Grootel, V., Charpinet, S., Fontaine, G., Green, E. M. & Brassard, P. Structural and core parameters of the hot B subdwarf KPD 0629–0016 from CoRoT *g*-mode asteroseismology. *Astron. Astrophys.* **524,** A63 (2010).
26. Charpinet, S. *et al.* Deep asteroseismic sounding of the compact hot B subdwarf pulsator KIC02697388 from *Kepler* time series photometry. *Astron. Astrophys.* **530,** A3 (2011).
27. Domìnguez, I., Höflich, P. & Straniero, O. Constraints on the progenitors of type Ia supernovae and implications for the cosmological equation of state. *Astrophys. J.* **557,** 279–291 (2001).

Acknowledgements S.C., N.G. and W.Z. acknowledge financial support from Programme National de Physique Stellaire (PNPS) of CNRS/INSU, France, and from the Centre National d'Études Spatiales (CNES, France). We also acknowledge support from the Agence Nationale de la Recherche (ANR, France) under grant ANR-17-CE31-0018, funding the INSIDE project. This work was granted access to the high-performance-computing resources of the CALMIP computing centre under allocation number 2017-p0205. This work was supported by the Fonds Québécois de la Recherche sur la Nature et les Technologies (FQRNT, Canada) through a postdoctoral fellowship awarded to N.G. G.F. also acknowledges the contribution of the Canada Research Chair Program, and W.Z. the LAMOST fellowship as a young researcher, supported by the Special Funding for Advanced Users, budgeted and administrated by the Center for Astronomical Mega-Science, Chinese Academy of Sciences. V.V.G. is an F.R.S.-FNRS Research Associate. The authors acknowledge the Kepler team and everyone who has contributed to making this mission possible. Funding for the Kepler mission is provided by NASA's Science Mission Directorate.

Author Contributions N.G. wrote the manuscript and performed the seismic analysis of KIC08626021. S.C. and G.F. contributed to the writing of the manuscript. S.C., P.Br. and N.G. contributed to the development of the numerical codes used in this analysis. E.M.G. obtained the spectroscopic data for KIC08626021. P.Be. and G.F. performed the model atmospheric analysis. W.Z. provided Fig. 1. V.V.G., G.F. and M.A.D. performed non-adiabatic complementary analysis. All authors discussed the results and contributed to their interpretation.

Author Information Reprints and permissions information is available at www.nature.com/reprints. The authors declare no competing financial interests. Readers are welcome to comment on the online version of the paper. Publisher's note: Springer Nature remains neutral with regard to jurisdictional claims in published maps and institutional affiliations. Correspondence and requests for materials should be addressed to N.G. (noemi.giammichele@irap.omp.eu).

Reviewer Information *Nature* thanks M. Salaris, O. Straniero and the other anonymous reviewer(s) for their contribution to the peer review of this work.

METHODS

Our method revolves around minimizing a merit function defined by the sum of the squared differences between theoretical and observed periods, in order to isolate an optimal self-consistent seismic model that best reproduces the oscillation properties of the star under consideration[20]. The method and tools used here are essentially the same as those used in the recent successful test[20] in the case of the pulsating ZZ Ceti stars GD 165 and Ross 548, except that we include the detailed parameterization of the chemical composition profile in the star's core[9]. The method is inspired by work on pulsating hot subdwarf stars[28], which has been developed further over the years[29–31]. Most recently, a discussion of our continuing quest for an objective approach to quantitative asteroseismology has been presented with application to white-dwarf stars in particular[10,32]. The forward approach used here consists of comparing the pulsation periods of large numbers of theoretical stellar models—defined by N free parameters—to the observed periods of the pulsating star of interest. By optimizing this process, it is possible to infer the structural parameters of the appropriate stellar model via the best fit to the observed period spectrum. Given that we have no preconceived idea of the mode identification (except for the fact that the observed periods are likely to have a degree index, l, of 1 or 2, in keeping with what is known about identified gravity modes in white dwarfs), the optimization process has to be twofold. The technique thus relies on a double-optimization scheme that, first, best matches the observed periods with the periods calculated from a theoretical spherical stellar model, using a χ^2-type formalism viewed as a combinatorial optimization problem. The first optimization therefore consists of finding the combination (or mode identification) that leads to the best possible simultaneous match of all the observed periods for that given model. It is based on a stochastic method using an evolutionary approach to optimization problems[32]. The method allows for the automatic and objective identification of modes, without any prior knowledge of the mode identification and outputs from the best fit, the degree l and the radial order k for each mode. The second optimization uses a multimodal optimizer based on a massively parallel hybrid genetic algorithm to find the best-fitting model in the N-dimensional parameter space, the quality of the fit being quantified by a merit function, S^2 (an unweighted χ^2):

$$S^2(a_1, a_2 \ldots, a_N) = \sum_{i=1}^{N_{\rm obs}} (P_{\rm obs}^{(i)} - P_{\rm th}^{(i)})^2 \qquad (1)$$

where $N_{\rm obs}$ is the number of observed periods; a_1, a_2, …, a_N are the parameters of the model; and each $P_{\rm obs}^{(i)}$, $P_{\rm th}^{(i)}$ is a pair of matched observed–theoretical periods for this model. The code used, named LUCY[30], performs a complete and exhaustive exploration of the entire model parameter space and gives feedback on the uniqueness (or not) of the solution. Some illustrations of the capabilities of the code and further details can be found in ref. 32.

Parameterized models. The evaluation of S^2 requires computation of a large number of theoretical stellar models from which we obtain the period spectra. This is best achieved through the use of static, parameterized equilibrium models[20]. Note that these are full stellar models (not envelope models), and that, for a cooling white dwarf, the well calibrated relation $L(r) \propto M(r)$ ensures a good description of the luminosity profile. To define a full, static V777 Her white-dwarf model, it is necessary to specify the surface gravity (or the mass via the mass–radius relation; we prefer to use the surface gravity because it allows direct comparison with atmospheric parameters derived from spectroscopy), the effective temperature, the envelope layering, the core composition and the convective efficiency. In the case of low-order, short-period g-modes such as those observed in KIC08626021, the periods are quite insensitive to the precise choice of the latter parameter (see, for example, figure 42 in ref. 17), so we fixed it to the 'flavour' ML2/$\alpha = 1.25$, as calibrated through DB spectroscopy[33].

For a DB star, the envelope layering must be defined by a minimum of five parameters. This is illustrated in Extended Data Fig. 2, which shows the general shape to be expected for the helium profile in such a star. The envelope is characterized by two zones: first, an upper pure-helium layer with a thickness specified by $\log(q_1)$, produced by the gravitational settling of carbon and oxygen in earlier evolutionary phases; and second, a lower mixed zone with a base located at $\log(q_2)$ and in which separation between helium, carbon and oxygen still goes on. The quantity $X(\mathrm{He})_{\rm env}$ indicates the helium mass fraction in the mixed zone and represents the atmospheric helium content in the presumed PG 1159 ancestor. These quantities are related in such a way that $\log(q_1)$ corresponds to the fractional mass depth at which the local value of the helium mass fraction is equal to $(1+X(\mathrm{He})_{\rm env})/2$, while $\log(q_2)$ corresponds to the depth where that mass fraction is equal to $X(\mathrm{He})_{\rm env}/2$. In addition to these three parameters, the stratification of helium in the envelope of a DB white dwarf must also be characterized by the actual shape of the profile in the composition transition zone between the pure-helium outermost layer and the flat portion of the curve in the mixed zone, as well as the shape of the corresponding transition profile between the mixed zone and the core, where $X(\mathrm{He})$ goes to zero.

To handle this problem, we first compute, for each transition zone, the actual profile obtained from the strict condition of diffusive equilibrium between ordinary diffusion and gravitational settling (we neglect the contribution of thermal diffusion here), which depends on the local conditions of density, temperature, and average charge of each ionic species of interest. Recognizing next that diffusive equilibrium cannot have been reached over the cooling lifetimes of DB white dwarfs, especially in the deeper regions of the star, we introduce a free parameter that acts as a multiplicative factor applied to the equilibrium profile. Varying that parameter—named P_1 for the upper transition zone and P_2 for the lower one—leads to a profile that may be steeper or shallower than the equilibrium one. The actual functional form used in this approach belongs to the so-called family of sigmoid functions. The implicit expression governing the chemical profile in such a transition zone is given by equation (1) of ref. 9.The parameters P_1 and P_2 have no particular physical meaning themselves. To summarize this, the envelope layering in a DB white dwarf model is defined by the specification of $X(\mathrm{He})_{\rm env}$, $\log(q_1)$, $\log(q_2)$, P_1 and P_2.

To describe the complicated chemical stratification expected in the core of a carbon–oxygen white dwarf, we adopt a seven-parameter description[9]. This follows from the realization that g-modes can sometimes be confined in the deep core of a cool white dwarf[20] (this was the case for Ross 548, but not for GD 165), and thus could serve as probes of that core. In ref. 20, it was crudely assumed for simplicity that the carbon–oxygen core is homogeneous in composition, so that it could be characterized by a single free parameter, the carbon/oxygen ratio. Although the chemical composition of the core of a carbon–oxygen white dwarf is not expected to be homogeneous according to stellar evolution theory, this simple approach at least leads to an estimate of the bulk composition in a case, such as that of Ross 548, where there are detected modes with non-negligible amplitudes and weight functions extending into the core. The lesson here is that we should be prepared *a priori* to exploit potentially confined modes of this sort.

Figure 1 of ref. 9 illustrates in a schematic way the proposed parameterization for the carbon–oxygen core of a typical white dwarf. Strictly speaking, that parameterization applies to the cores of hydrogen-atmosphere, or DA, white dwarfs. For a DB star, an eighth parameter should be added; that is, the value of $X_{\rm env}(\mathrm{O})$ at the outer boundary of the core should not be set to zero as is the case for a DA star, but to some value, variable from one object to another, that reflects the atmospheric oxygen content in the previous PG 1159 evolutionary phase. This atmospheric pollution is the direct consequence of the violent mixing event that is associated with the born-again scenario at the origin of helium-atmosphere white dwarfs. As discussed in detail in ref. 9, eight control points are necessary to fully define a two-transition chemical profile in the core of a DB white dwarf. These control points correspond to the following parameters: core O, $t1$, $\Delta t1$, $t1(\mathrm{O})$, $t2$, $\Delta t2$, $t2(\mathrm{O})$ and $X_{\rm env}(\mathrm{O})$ (see figure 1 of ref. 9). The flexibility of our parameterization allows us to also test different structural configurations during the same process; for example, we can obtain and test a single-layered envelope when $q_1 = q_2$, or a single-transition chemical profile in the core by only using the subset of core O, $t1$ and $\Delta t1$, and by setting $t1(\mathrm{O})$ and $t2(\mathrm{O})$ to 0.

In the end, we carry out our search in parameter space by optimizing a total of 15 parameters: the surface gravity, the effective temperature, the five quantities defining the helium-rich envelope, and the eight parameters characterizing the carbon–oxygen core. Once the structure is fully defined, the following step is to evaluate the adiabatic pulsation properties of the model—assumed to be purely spherical—using an efficient and robust code based on finite-element techniques[34,35].

Pulsation properties. To carry out our seismic study, we use a recent thorough analysis[18], which has shed new light on the 23 months of Kepler photometric data gathered for KIC08626021. In particular, even if the 13 retained frequencies are consistent with previous analyses[21], interpretation of one of the structures leads to an important correction. The structure in the 3,677–3,686 μHz range, identified previously as a triplet[21,36], is actually a doublet, f_3 (ref. 18), with an independent mode, f_7, close by. The seismic modelling is greatly influenced by the addition of this eighth low-order frequency, as it must probe a somewhat different part of the star than the other modes, thus adding to the total information content available from the observations and contributing to a more detailed seismic view of KIC08626021. The list of extracted periods (frequencies) and their specifications are provided in table 1 of ref. 18; we refer the reader to this work for details of the extraction process and the frequencies detected. We use the same convention for the sake of simplicity.

Our seismic analysis is thus based on the following eight frequencies: f_1, f_2, f_3, f_4, f_5, f_6, f_7 and f_9. There is fine structure around three of these peaks in the Fourier domain: f_1 and f_2 are two clearly identified and nearly symmetric triplets in frequency space, while f_3 shows a doublet structure with components separated by a spacing comparable to those seen in the triplets. Interpreted as rotational splitting, this fine structure corresponds to a rotation timescale of about 42.5 h

if the three modes are assumed to be dipole modes and if the asymptotic expression for the first-order solid-body rotation coefficient, C_{kl}, is used: that is, $C_{kl} = 1/(l^2 + l) = 0.5$. Out of the remaining four periodicities listed in table 1 of ref. 18, f_8 and f_{10} are linear-combination frequencies of two of the eight basic modes, and as such, they are excluded from our analysis. In addition, we do not consider f_{11} and f_{12} because they do not reach the secure threshold of 5.6σ (ref. 18).

The optimal model. The search for best-fitting solutions starts with the largest possible parameter space for DBV stars. Constraints on $T_{\rm eff}$ and $\log(g)$ rely on typical spectroscopic values found for DBV stars, being as inclusive as possible. Evolutionary tracks[2] influenced the search ranges for the eight parameters defining the C–O core: core O, $t1$, $\Delta t1$, $t1$(O), $t2$, $\Delta t2$, $t2$(O) and $X_{\rm env}$(O). We consider all modes of degree $l = 1$ and $l = 2$ in the period range from 100 s to 500 s, which encompasses the range spanned by the eight main observed modes in KIC08626021. Modes with higher degree are excluded, as we expect them to be hardly visible owing to cancellation effects of their surface geometry. We thus searched parameter space in 15 dimensions in order to best fit eight periods. *A priori*, this seems like an underconstrained problem, but this simplistic point of view is in fact incorrect in the context of the present optimization exercise—a highly nonlinear problem. This point has been discussed at length[9,10].

Keeping this in mind, we singled out a model in parameter space that can match the observed periods at an unprecedented level of precision, defined by a merit function of $S^2 = 1.4 \times 10^{-15}$. Information on the best-fitting model—including details of the period spectrum and mode identification—is presented in Extended Data Table 1. This very precise seismic match reaches (for the first time, to our knowledge) the actual observational limit. In this case, the observational limit is $\Delta P = 0.000038$ s or $\Delta\nu = 0.00060\,\mu$Hz, based on the two years of Kepler data on KIC 08626021—justifying the number of digits given in Extended Data Table 1 for these quantities.

Extended Data Fig. 3 shows a projection map of the merit function onto the $T_{\rm eff}$–$\log(g)$ plane. The merit function is normalized in such a way that the global minimum is equal to one, on a logarithmic scale. As can be seen, the seismic effective temperature falls well within the spectroscopic 1σ box. The seismic value of $\log(g)$ is also in excellent agreement with the spectroscopic determination to within 1σ. The actual seismically inferred values of $T_{\rm eff}$ and $\log(g)$, along with the other defining parameters for this unique solution, are listed in Extended Data Table 2.

The pure He layer is rather thin with a value of $\log(q_1) = -7.63$, representing the position of the transition between the mixed-composition envelope and the pure He layer in the $\log(q)$ coordinate. The envelope composed of a mixture of oxygen, carbon and helium, with a global mass fraction of 18.1% He, is defined by $\log(q_2) = -3.23$. This leads to a total helium mass fraction (integrated over the full model) of $\log[M({\rm He})/M_*] = -3.948$ or, equivalently, $M({\rm He})/M_* = 0.0113\%$. Using the global and shape parameters listed in Extended Data Table 2, we report our primary results in Table 1 (these results are the top 11 entries in the table and include the total mass, which is a direct product of the constitutive physics used in our stellar models). From those, one can infer interesting secondary quantities such as the radius, the luminosity, the absolute magnitude in the Sloan Digital Sky Survey (SDSS) r-band, and an estimate of the distance to KIC08626021. Other secondary properties, reported in the lower part of Table 1, can also be inferred as discussed below.

An integral part of our approach is the requirement that the neighbourhood of the optimal model in parameter space be thoroughly explored in order to assess the statistical significance of the solution and to provide estimates of uncertainties on each derived parameter. As an example, Extended Data Fig. 4 shows the histograms obtained for the probability distribution of six interesting parameters used during the present optimization. The technique used relies on the likelihood function calculated from the sampling of the merit function S^2 during the search for the best-fitting model. This method[31] allows us to make more quantitative statements on the value of each parameter by statistically estimating that value and its associated errors from the seismic fit[20]. We also incorporate in the error budget, at least partially, an evaluation of external errors resulting from potential systematics. In a nutshell, all of the histograms show narrow peaks, with the mean and median values of the distribution being very close to each other. The derived uncertainties are listed in Table 1.

The inferred chemical stratification. Our central result is the unravelling of the complex internal chemical stratification of KIC08626021 (see Fig. 2). The 1σ uncertainties in Fig. 2 (the shaded areas) are derived from the probability distributions calculated during the optimization process. For completeness, we show, in Extended Data Fig. 5, the individual normalized probability distributions for oxygen, carbon and helium obtained during this exercise.

We also point out that our ability to probe the core composition is intimately associated with the presence of detected modes with amplitudes and weight functions sufficiently important in the core for the pulsation periods to show a sensitivity to the local chemical composition and stratification[20]. Extended Data Fig. 6a illustrates that all of the eight modes of interest in our optimal seismic model (those identified with the eight observed pulsations) have at least some sensitivity to the core structure, as measured by the non-negligible values of their weight functions at those depths. Some of the modes, such as those with $l = 1$, $k = -3$ and $l = 2$, $k = -4$ (that is, the confined modes), are particularly good probes of the core composition[20].

In comparison with the much cooler ($T_{\rm eff} \approx 12{,}000$ K) ZZ Ceti stars[20] (see figure 6 of ref. 20 in particular), we find that the capacity of seismic waves to sound the core structure of a hot V777 Her pulsator such as KIC08626021 is much higher. This is explained by the well known effect of amplitude-mode migration associated with increased overall degeneracy in the cooler ZZ Ceti stars, which pushes outwards, and away from the core, the non-negligible parts of the weight function (see, for example, figure 8 of ref. 17).

Comparison with previous studies. It is also appropriate to compare our seismic results with those obtained in previous (adiabatic) studies dedicated to KIC08626021. Following the report of the discovery of five distinct pulsation modes in this star on the basis of one month of Kepler photometry[8], three different groups presented preliminary seismic analyses. The first study[37] made use of parameterized evolutionary models computed with the white dwarf evolution code (WDEC). Five defining quantities were varied: the effective temperature, the total mass, two parameters characterizing the core, and one free parameter describing the envelope. Following this, an independent seismic study[38] was carried out based on evolutionary models with a full history from the zero-age main-sequence (ZAMS). In principle, such models are the most realistic ones available and are defined only by the total mass and initial chemical composition.

However, by design, these models show no flexibility in how they treat a star's constitutive physics, and they hide defects, including accumulated numerical noise and artefacts (see ref. 20 for the need for parameterized models in white-dwarf seismology). The third investigation[39] used an earlier version of the approach we use here, with the big difference that there was no detailed core parameterization. The core was assumed to be homogeneous in composition and characterized by a single quantity, the carbon-to-oxygen ratio. Specifying the effective temperature, the surface gravity, and a three-parameter description of the envelope, these authors[39] searched a six-dimensional parameter space using full, but static models. They obtained two solutions, the first assuming that all five modes are dipole modes, and the second allowing the possibility that the modes belong to degree index $l = 1$ or 2. Finally, the addition of two newly uncovered frequencies from the extended dataset[36] motivated another attempt at deciphering KIC08626021 (ref. 21), again with the use of parameterized evolutionary models computed with WDEC. In this case, an additional parameter (making a total of six) was included in the search in parameter space, in order to provide a more flexible description of the envelope. Two possible solutions were presented[21].

As a first step, we contrast the mode identification and the normalized merit function of each of the previous studies with our work in Extended Data Table 3. The normalized merit function, s^2, is defined as the merit function presented in the equation above, divided by the number of fitted periods. It allows us to put all seismic studies on KIC08626021 on the same footing for purposes of comparison. Note that our work is based on reanalysis of the nearly two years of Kepler data, which added an extra frequency[18] to the frequency spectrum used by the most recent study[21]. We also note that to fit simultaneously an increased number of observed periods is a more demanding challenge, especially when they are low-order modes, because they contain extra information about the pulsating star and are sensitive to any small change in the modelled structure of the star. The resulting parameter space becomes more intricate and complex to resolve.

From Extended Data Table 3, we find it reassuring that the mode identification appears to be quite robust. Indeed, except for the case of the mode with a period of 376.11 s, all of the different seismic analyses lead to the same values of l and k for the observed periods. In the former case, the proposed identification has been either $l = 1$ and $k = 8$, or $l = 2$ and $k = 15$ (which are our derived values). Note that the identification of $l = 1$ and $k = 8$ for the 376.11 s pulsation in solution 1 of ref. 39 is 'artificial' in the sense that only dipole modes were considered in the period-matching exercise. By letting the five pulsations available free to be $l = 1$ or $l = 2$ modes, these authors obtained a much improved fit, including the identification of $l = 2$ and $k = 15$ for the 376.11 s period (their solution 2).

In terms of the quality of the fit, as measured by the normalized merit function, Extended Data Table 3 reveals a clear correlation between the method used and the results obtained. Considering first the three initial analyses based on the detection of five pulsations, we find that, first, the standard method of using detailed evolutionary models[38] gives a poor fit to the observed periods ($s^2 = 3.74$); second, a much improved fit ($s^2 = 7.84 \times 10^{-2}$) is obtained when using parameterized evolutionary models[37]; and third, a further improved fit ($s^2 = 2.51 \times 10^{-5}$) is obtained when using parameterized static models[39]. We believe that this 'progression' is notable in that the latter method is the most optimized one for searching parameter space in

fine detail. While solution 2 of ref. 39 shows a good fit to the observed periods, the computed periods still do not match the precision of the observations. On can conclude from this that a complicated object such as KIC08626021 cannot be modelled precisely in terms of six parameters only. By comparison, we have been able to fit essentially perfectly ($s^2 = 1.75 \times 10^{-16}$) the eight periods now detected in that star. This orders-of-magnitude improvement is the direct result of the flexibility of our new parameterization, coupled with an efficient algorithm that finds the optimal solution and evaluates finely the shape of the merit function in parameter space.

Extended Data Table 4 lists the main parameters defining the structure of our white-dwarf model compared with results from previous studies. Note that $\log(q_1)$ corresponds to $M_{\rm He}$, $\log(q_2)$ corresponds to $M_{\rm env}$, and $\log(q_3)$ is directly linked to $q_{\rm fm}$ (refs 21, 37). These two studies make use of the same parameterization, with the only difference being that $M_{\rm env}$ was kept fixed during their first attempted seismic analysis. The chemical structure found for the core and envelope[38] is kept fixed according to their predictions from evolutionary computations, but they give the values of these three reference points for comparison purposes.

Inferences of the global parameters $T_{\rm eff}$ and $\log(g)$ (mass) are all within 1σ of the spectroscopic values, except for a specific analysis[38]. Reference points from the He-envelope layering—$\log(q_1)$ and $\log(q_2)$—are also similar in values. The main differences arise from the core definition $\log(q_3)$ and $X(\rm O)_{\rm central}$, where our solution presents an extended central carbon–oxygen core as well as a higher composition in oxygen in this homogeneous part.

Spectroscopic constraints. The first analysis of the time-averaged optical spectrum of KIC08626021 revealed the DB nature[8] of this relatively faint star at a Kepler magnitude, $K_{\rm p}$, of 18.46. These authors used a low signal-to-noise ratio (S/N) classification spectrum gathered with the intermediate-dispersion spectrograph and imaging system (ISIS) on the William Herschel Telescope, combined with spectroscopic model grids[40]. The mixing-length (ML) prescription of ML2/$\alpha = 1.25$ for DB models[33] was adopted. The standard fitting procedure[41] gave $T_{\rm eff} = 24{,}900 \pm 750$ K and $\log(g) = 7.91 \pm 0.07$. Of these two preliminary estimates, that of the effective temperature revealed itself somewhat suspect, given that KIC08626021 belongs to the shortest-period pulsators of all of the known V777 Her stars and, therefore, has to be among the hottest of the class according to the well known period–luminosity relation depicted, for example, in figure 25 of ref. 17. Hence, the true effective temperature of KIC08626021 has to be much higher than the estimate provided[8], which is more characteristic of the red edge of the V777 Her instability strip[42]. The need for a better optical spectrum of KIC08626021 was subsequently emphasized[37] because of the apparent conflict between the initial spectroscopic estimate of the effective temperature and the seismic model, which indicated a value of $T_{\rm eff} \approx 29{,}200$ K.

Shortly after the variability of KIC08626021 was reported, we obtained a better spectrum with the help of the Bollers and Chivens Cassegrain spectrograph attached to the Steward Observatory's 2.3-m Bok Telescope on Kitt Peak. Seven individual spectra, each with an exposure time of 1,800 s, were gathered on 26 June 2011 (universal time). We used the 400 mm^{-1} first-order grating with a 2.5″ slit to obtain a spectrum with a typical resolution of about 8.7 Å over the wavelength interval 3,620–6,900 Å. The instrument rotator was set before each exposure, in order to align the slit within about 2° of the parallactic angle at the midpoint of the exposure. Helium–argon comparison spectra were taken immediately after the stellar exposure. The spectra were bias-subtracted, flat-fielded, background-subtracted, optimally extracted, wavelength-calibrated, and flux-calibrated using standard image reduction and analysis facility (IRAF) tasks. They were then shifted to the same relative velocity before being combined into a single spectrum (although the velocity differences between the seven spectra were unsubstantial). The total exposure time was 12,600 s, much larger than the periods of the detected pulsations (which all have low amplitudes of less than 1% of the mean brightness of the star), thus ensuring that the combined spectrum is representative of the mean effective temperature and surface gravity. The combined spectrum has a mean value for S/N of around 50, which is excellent for a faint star such as KIC08626021.

Two of us presented a preliminary analysis of that time-averaged spectrum[39]. More recently, using the same technique[12], we repeated the spectroscopic analysis. Our updated fit is presented in Extended Data Fig. 1. The fit to the available lines is quite good, and leads to the following atmospheric parameters: $T_{\rm eff} = 29{,}360 \pm 780$ K, $\log(g) = 7.89 \pm 0.05$, and $\log(\rm H/He) = -3.0 \pm 0.1$. Interestingly, we detect a small trace of hydrogen, making KIC08626021 one of the hottest known DBA white dwarfs. At the same time, and more importantly in this context, our revised estimate of the effective temperature also makes KIC08626021 the second hottest of the known V777 Her pulsators (as it should be on the basis of its short observed periods). Pulsation was confirmed[43] for the known DB star PG 0112+104, from the K2 dataset, making it the hottest known V777 Her pulsator, with a most recent estimate of $T_{\rm eff} = 31{,}040 \pm 1{,}060$ K (ref. 12). In our seismic analysis, the spectroscopic estimates of $T_{\rm eff}$ and $\log(g)$ are used as important independent constraints. Any seismic model to be found must be compatible with these constraints in order to be credible. We note in this context that our spectroscopic analysis is perfectly compatible with an independent study carried out[44] on the basis of Cosmic Origins Spectrograph (COS)/Hubble Space Telescope (HST) spectroscopy and of SPY optical data. These authors infer the values of $T_{\rm eff} = 30{,}000 \pm 1{,}000$ K and $\log(g) = 7.89 \pm 0.15$ for KIC08626021, solidifying the spectroscopic constraints used here.

Internal rotation profile. Given a seismic model, it is possible to exploit the fine structure uncovered by Kepler in three of the eight main modes detected in KIC08626021 (ref. 18). Interpreted as rotational splitting, the triplet structures seen in the $l = 1$, $k = -3$ (197.1 s) and in the $l = 1$, $k = -4$ (232.0 s) pulsations, as well as the doublet seen in the $l = 1$, $k = -5$ (271.6 s) pulsation, can be used to infer the internal rotation profile of KIC08626021, or part of it. This is different from the usual approach (as used above) for estimating a rotation timescale only on the basis of the detected spacings within frequency multiplets. In that case, there is no information whatsoever on the location at which the rotation timescale originates. Instead, it is possible to probe the actual rotation profile as a function of depth[20,30,45].

The rotation kernels associated with each of these three frequency multiplets were computed on the basis of our optimal model and our mode identification. These functions play a similar role to the weight functions encountered above, except that they indicate the regions inside a model at which the local rotation law can be probed (or not). In the present case, we find that the outer 70% or so of the radius can be sounded for rotation. This corresponds to the outer roughly 81% of the mass of the star. Our results are summarized in Extended Data Fig. 6b. We find that the available multiplet data are compatible with the proposition that KIC08626021 rotates rigidly over its outer 70% or so in radius with a period of $P_{\rm rot} = 46.34 \pm 2.54$ h. Given the available limited rotation data, we cannot exclude the possibility of some mild differential rotation about that value, but the most important result is that the star rotates globally (over at least 81% of its mass) very slowly by stellar standards. This adds to mounting evidence[46] that isolated white dwarfs have lost most of their initial angular momentum.

We can combine the value of the rotation period, $P_{\rm rot}$, with our seismic estimate of the radius, R_*, of KIC08626021 to derive its equatorial velocity, $V_{\rm eq}$, as follows: $V_{\rm eq} = 2\pi R_*/P_{\rm rot}$. Likewise, assuming that the star rotates rigidly over its full extent, from centre to surface, we can obtain a value for its total angular momentum, J, which is some 291 times smaller than the total angular momentum of the Sun (a future white dwarf). We report these data in Table 1. In terms of energy, these data correspond to a ratio of the total rotation energy of KIC08626021 to its internal energy of $E_{\rm rot}/E_{\rm th} = 8.11 \times 10^{-8}$, which is another way of demonstrating that rotation plays a negligible role in the further evolution and structure of this star.

Further observables. The potential of a hot V777 Her star such as KIC08626021 to serve as a benchmark for measuring plasmon neutrino emission is well known[47]. Long-term efforts and stable pulsation frequencies are required in order to measure reliable values for the rates of period changes, $\mathrm{d}P/\mathrm{d}t$, associated with the secular evolution (cooling) of the star. Although the task appears difficult for KIC08626021 owing to its faintness ($K_{\rm p} = 18.46$), we nevertheless decided to provide estimates of rates of period changes for the three highest-amplitude modes observed in that star. These may be useful in the future.

We thus computed two evolutionary sequences incorporating the detailed chemical profile inferred from our seismic analysis, one with neutrino losses included (as in a standard calculation) and the other without. The rates of period changes were computed directly from each of these sequences (Table 1). For each of the three retained modes (identified by their periods), we list the expected value of $\mathrm{d}P/\mathrm{d}t$ with or without neutrino losses.

Excitation of the pulsation modes. It is obviously important to verify whether the pulsation modes of interest identified in the optimal model are indeed predicted to be excited through detailed stability calculations. For this, we use the Liège non-adiabatic code MAD[48], which takes properly into account the perturbations of the convective flux[49]. As it is, with the optimal model obtained with the same convective efficiency of ML2/$\alpha = 1.25$ as used in the spectroscopic analyses of DB/DBA white dwarfs, we find no unstable modes. That is, the optimal model is located above the ML2/$\alpha = 1.25$ blue edge for dipole modes in the $T_{\rm eff}$–$\log(g)$ diagram.

This situation is entirely analogous to the case of the cooler ZZ Ceti stars, for which it was found necessary to use a higher convective efficiency[50] in the pulsation models (the ML2/$\alpha = 1.0$ version) than that calibrated and used in the spectroscopic analyses (ML2/$\alpha = 0.6$) in order to best match the theoretical instability strip with the empirical (spectroscopic) one. The explanation is that the 'equivalent ML convective efficiency' increases with depth in white dwarfs, from the atmosphere down to the bottom of the convection zone, as demonstrated by detailed three-dimensional hydrodynamic calculations and recent calibration efforts[51].

In the same way as for the ZZ Ceti stars[50], we examined the stability properties of models in all points similar to the optimal seismic model, but with an increased convective efficiency compared with the one used in the spectroscopic analyses.

Specifically, we considered ML2/$\alpha = 1.5$ and ML2/$\alpha = 1.6$. This is discussed above, but we recall here that the pulsation periods are quite insensitive to the choice of the convective efficiency in our models, while the driving and excitation of modes depend quite sensitively on the location of the base of the effective convection zone, a quantity that depends intimately on the choice of the convective efficiency.

Some of our results are presented in Extended Data Fig. 6c, which illustrates the ranges of detected periods in relation to the bands of predicted unstable modes. In particular, we find that a convective efficiency with the ML2/$\alpha = 1.6$ flavour is required to drive all of the eight observed modes in our model of KIC08626021. Additional calculations indicate that, for that particular efficiency (and for a total mass of $0.570 M_{\odot}$), the blue edge of the V777 Her instability strip is located near $T_{\rm eff} \approx 31{,}190$ K for the dipole modes, and around $T_{\rm eff} \approx 32{,}090$ K for the quadrupole modes. This is probably sufficient also to account qualitatively for the presence of pulsations in the hottest known V777 Her pulsator, PG 0112+104 (ref. 43).

In short, and in retrospect, our extensive search for an optimal model in parameter space should have been done with a convective efficiency of, for example, ML2/$\alpha = 1.6$, to ensure a better consistency between adiabatic and non-adiabatic properties. However, for the reasons given above (mostly the insensitivity of the pulsation periods to the convective efficiency), we do not expect that the inferred chemical stratification would be much different to what we obtained should a new search be carried out. To be more precise, because this source of systematics has been considered in our evaluation of the error budget, any potential shift in the seismic solution is most likely within the conservative error estimates provided here.

Systematics. The procedure[9,20] introduced to evaluate uncertainties represents, by definition, internal errors of the fit propagated to the derived parameters. Here, these internal errors are in fact very small, owing to the very high precision achieved in measuring the pulsation periods by the Kepler spacecraft and in matching the periods at this precision with a model. However, the internal chemical profile and global parameters inferred here do depend specifically on the particular components of the constitutive physics that went into our model building—an additional source of uncertainty that we call systematics or external errors. That is, the results must be sensitive to, for example, our choice of radiative opacity, conductive opacity, and equations of state for the fully ionized interior as well as the partially ionized non-ideal envelope. For example, had we used the Opacity Project (OP) radiative opacities instead of the OPAL data in our model codes, the inferred chemical profile would necessarily have been different. It is difficult to assess by how much, although we would expect only relatively small differences because the two sets of opacities have proven very similar, especially for the light elements such as hydrogen, helium, carbon and oxygen. To be more quantitative at this point would require a major computational effort (we would need to carry out many further full searches in parameter space, which is not feasible); such an effort will have to wait for the future, if deemed necessary. But other sources of systematics can be investigated in a more practical way and we discuss some of them below.

A more realistic core composition for a white dwarf should include a trace of neon-22, which is expected to be the most abundant of the minor species that must be present. Our approach to describing both the core and the envelope of a white dwarf has been limited to four elements—hydrogen, helium, carbon and oxygen—for which we have detailed, state-of-the art tabular data covering the full density–temperature range of interest for the equation of state (liquid and solid phases), radiative opacity, and conductive opacity. These are the elements that leave a dominant seismic signature on the run of the Brunt–Väisälä (BV) frequency (because we are dealing with gravity modes), and, therefore, their abundances are the most easily measured through seismic analysis. In this context, we find that the presence of neon-22, in trace form, has no direct imprint on the BV frequency profile. Indeed, an examination of the neon-22 profile in figure 9 of ref. 52 indicates an essentially flat distribution, with a mass abundance of $X(^{22}\mathrm{Ne}) = 0.02$ from the centre outwards to a $\log(q)$ of around -5 for their representative $0.5885 M_{\odot}$ model of a white dwarf. Figure 5 of ref. 5 shows a similar result for their $0.64 M_{\odot}$ model of a carbon–oxygen white dwarf calculated with the Modules for Experiments in Stellar Astrophysics (MESA) code. The profile of neon-22 being flat, its chemical signature on the BV frequency is limited only by the absolute value of that frequency, not by a composition 'spike' that would constitute a telltale sign of its presence. Given the small absolute abundance of neon-22, its presence will probably remain undetectable through seismic means.

Nonetheless, the (probable) presence of neon-22 must affect the pulsation periods, but the effect is certainly small *a priori*. It resides in the difference in constitutive physics between a dominant element, say oxygen, and the isotope neon-22. This difference can be seen as a correction to a correction, given the small abundance of that element to start with. We expect that neon-22's largest effect is to cause a difference in the equation of state, through the effects of Coulomb interactions between the ions. The addition of a trace of neon-22 in a model 'softens' the equation of state; that is, for a given mass the radius will be slightly smaller. This implies that the pulsation periods will systematically decrease by some small amount because the average density is slightly boosted.

The other effect comes from the conductive opacity (the radiative opacity of neon-22 is not important here, because neon-22 is present only in the degenerate core, where electron conduction dominates the energy-transfer process). Because of the larger average charge carried by neon-22 ions compared with, say, oxygen ions, we expect a slight increase in the global conductive opacity. This leads to a very small increase in the temperature, which reduces the pulsation periods of gravity modes in white dwarfs. This second phenomenon, a thermal effect, goes in the same direction—that is, a decrease in the pulsation periods—but it is less important than the first phenomenon, a mechanical effect. With some effort, we have been able to put these considerations on a firm quantitative basis. First, we computed an appropriate sophisticated equation of state for neon-22 that applies to the cores of white dwarfs, using a code developed at Université de Montréal[53]. To our knowledge, this is the first detailed equation of state computed for an isotope such as neon-22. Next, we used the old conductive opacity code[54] to estimate the differences in conductive opacity between neon-22 and a reference element, which we take as oxygen. We note that we do not use the old Hubbard–Lampe conductive opacities in our model-building code. Instead, we use the latest upgrades[55] for hydrogen, helium, carbon and oxygen. Because a Potekhin version of the conductive opacity of neon-22 is not readily available, we resorted to the Hubbard–Lampe code to estimate in a differential sense the conductive opacity of neon-22 with respect to that of oxygen. We find that the conductive opacity of neon-22 is some 1.19 times larger than that of oxygen-16, averaged over the density–temperature domain of interest for our models of KIC08626021, that is, $6.8 < \log(T) < 7.9$, and $2.0 < \log(\rho) < 6.5$.

The next step was to build a standard reference model using a simple structure for a DB white dwarf: a pure oxygen core surrounded by a pure helium mantle. This was computed for a mass and an effective temperature equal to those inferred for KIC08626021. We pulsated that structure with our high-precision, finite-element adiabatic pulsation code and noted the pulsation periods. Next, we computed another similar DB equilibrium structure, except that the pure oxygen core was replaced by an oxygen-dominated core with a trace of neon ($X(^{22}\mathrm{Ne}) = 0.02$) from the centre outwards to $\log(q) = -5$, following predicted evolutionary models[52].

To do this, we 'fooled' our model-building code into 'thinking' that oxygen is carbon, while neon-22 is oxygen. That is, we replaced all of the constitutive physics appropriate for carbon by that of oxygen (equation of state and opacities), while we replaced the equation-of-state tabular data for oxygen with our new results for neon-22, and multiplied the modern (Potekhin) value of the conductive opacity of oxygen by the factor 1.19 described above.

As expected, there is no noticeable difference between the two models. The presence of neon-22 at the abundance used would not be revealed through seismology. However, as indicated above, we do find some tiny systematic differences in the absolute value of the BV frequency, which lead to slight differences in pulsation periods. Using the eight modes identified herein, we find that, on average, the pulsation periods are shorter by 0.34 s compared with the average period of 254.4 s, leading to a 0.1% effect—as expected, quite small. This comparison also confirms that most of the decrease in pulsation period is due to the difference in the equation of state; this is the main source of systematic errors. Given that a 0.1% shift in the periods of the optimal model translates into a S^2 value of about 0.12 for the period fit, we incorporated this value as a local minimal threshold of the merit function to compute the likelihood distribution, so the error estimates now reflect the impact of this external factor.

To test our specific choice of the convective efficiency ML2/$\alpha = 1.25$, we computed a model in all points similar to the optimal one found here, except that we adopted a reduced efficiency specified by the flavour ML2/$\alpha = 1.0$. The most important effect of this is to move the base of the outer helium convection zone from $\log(q) = -2.506$ to $\log(q) = -13.222$. Although this is important for non-adiabatic calculations because the driving engine is located at the base of the convection zone in a pulsating white dwarf of the V777 Her type, the pulsation periods are hardly affected given that the weight functions for the modes of interest have practically negligible amplitudes in these outermost layers. This expectation is explicitly verified by comparing the periods corresponding to the eight modes of interest in the two models. We find that the pulsation periods in the ML2/$\alpha = 1.0$ model are systematically and almost uniformly reduced by 0.0025% compared with those of the optimal (ML2/$\alpha = 1.25$) model. This is in line with the results depicted in figure 42 of ref. 17, which shows a small but nevertheless systematic increase in the pulsation period of a mode with increasing convective efficiency. We note that such small differences are still much larger than the precision of the Kepler data used here, meaning that a fully fledged search in parameter space would again be needed to fully measure the dependence of the inferred profile. This computed error budget is included in the estimate of our systematics.

Similar considerations can be made when addressing the issue that KIC08626021 is not really a pure DB white dwarf, but has an atmosphere that contains a small trace of hydrogen ($\log(\mathrm{H/He}) = -3.0 \pm 0.1$), as indicated in our analysis of its optical spectrum. A more realistic model of KIC08626021 is that of a DBA star that contains that small trace of hydrogen in the outer convection zone. As above, we computed an extra model, similar in all points to our optimal model, but containing such a trace. This changes somewhat the structure of the convection zone, including a small shift of its base from $\log(q) = -12.506$ to $\log(q) = -12.533$. The effects are not negligible as far as the structure of the atmosphere itself is concerned. Indeed, because of the atmospheric opacity of hydrogen, there are differences between DB and DBA model atmospheres[12]. But the consequences are again practically negligible as regards the pulsation periods because, as pointed out above, the weight functions have practically negligible amplitudes in the outer convection zone. Specifically, we find that the pulsation periods in the DBA model are systematically and almost uniformly reduced by 0.0010% compared with those of the optimal (DB) model. Incorporating these systematic errors as an external source in the computed error budget is done as before.

We also tested the impact of parameters that control how the adiabatic pulsation periods are computed, but we found this source of systematics to be much smaller than those discussed above. In the same vein, calculations of the non-adiabatic periods of the optimal model showed that non-adiabatic effects on the periods themselves are so small that they are irrelevant as a source of systematics in our results.

In summary, the error estimates that we provide with the derived parameters and chemical composition profiles include internal errors of the fit and a conservative estimate of the identified, most prominent sources of relevant external uncertainties. Of course, further systematics of yet unknown nature cannot be ruled out. The best means of identifying them will be to compare the properties of the seismic model with independent measurements of the stellar properties. We recall that the independent spectroscopic measurements of $\log(g)$ and T_{eff} do match well with the seismic solution, suggesting that other possible systematic errors are likely to be small. Further tests of solution accuracy should become possible when the full data from the GAIA global space astrometry project become available.

Code availability. We have opted not to make publicly available the highly specialized numerical codes used here because of their complexity.

Data availability. The data that support the findings of this study are available from the corresponding author upon request.

28. Brassard, P. *et al.* Discovery and asteroseismological analysis of the pulsating sdB star PG 0014+067. *Astrophys. J.* **563,** 1013–1030 (2001).
29. Charpinet, S., Fontaine, G., Brassard, P., Green, E. M. & Chayer, P. Structural parameters of the hot pulsating B subdwarf PG 1219+534 from asteroseismology. *Astron. Astrophys.* **437,** 575–597 (2005).
30. Charpinet, S. *et al.* Testing the forward modeling approach in asteroseismology. II. Structure and internal dynamics of the hot B subdwarf component in the close eclipsing binary system PG 1336-018. *Astron. Astrophys.* **489,** 377–394 (2008).
31. Van Grootel, V., Charpinet, S., Brassard, P., Fontaine, G. & Green, E. M. Third generation stellar models for asteroseismology of hot B subdwarf stars. A test of accuracy with the pulsating eclipsing binary PG 1336-018. *Astron. Astrophys.* **553,** A97 (2013).
32. Charpinet, S., Giammichele, N., Brassard, P., Van Grootel, V. & Fontaine, G. Method and tools for an objective approach of white dwarf asteroseismology. *Astron. Soc. Pac. Conf. Ser.* **493,** 151–155 (2015).
33. Beauchamp, A. *et al.* Spectroscopic studies of DB white dwarfs: the instability strip of the pulsating DB (V777 Herculis) stars. *Astrophys. J.* **516,** 887–891 (1999).
34. Brassard, P., Pelletier, C., Fontaine, G. & Wesemael, F. Adiabatic properties of pulsating DA white dwarfs. III—a finite-element code for solving nonradial pulsation equations. *Astrophys. J. Suppl. Ser.* **80,** 725–752 (1992).
35. Brassard, P. & Charpinet, S. PULSE: a finite element code for solving adiabatic nonradial pulsation equations. *Astrophys. Space Sci.* **316,** 107–112 (2008).
36. Østensen, R. H. Nine months of monitoring of a V777-Her pulsator with the Kepler spacecraft. *Astron. Soc. Pac. Conf. Ser.* **469,** 3–7 (2013).
37. Bischoff-Kim, A. & Østensen, R. H. Asteroseismology of the Kepler field DBV white dwarf. It is a hot one. *Astrophys. J.* **742,** L16 (2011).
38. Córsico, A. H., Althaus, L. G., Miller Bertolami, M. M. & Bischoff-Kim, A. Asteroseismology of the Kepler V777 Herculis variable white dwarf with fully evolutionary models. *Astron. Astrophys.* **541,** A42–A50 (2012).
39. Brassard, P. & Fontaine, G. The case of the Kepler DBAV star J1929+4447. *EPJ Web Conf.* **43,** 05010 (2013).
40. Koester, D. White dwarf spectra and atmosphere models. *Mem. Soc. Astron. Ital.* **81,** 921 (2010).
41. Bergeron, P., Saffer, R. & Liebert, J. A spectroscopic determination of the mass distribution of DA white dwarfs. *Astrophys. J.* **394,** 228–247 (1992).
42. Van Grootel, V., Fontaine, G., Brassard, P. & Dupret, M.-A. The theoretical instability strip of V777 Her white dwarfs. *Astron. Soc. Pac. Conf. Ser.* **509,** 321 (2017).
43. Hermes, J. J. *et al.* A deep test of radial differential rotation in a helium-atmosphere white dwarf. I. Discovery of pulsations in PG 0112+104. *Astrophys. J.* **835,** 277 (2017).
44. Koester, D., Provencal, J. & Gänsicke, B. Atmospheric parameters and carbon abundance for hot DB white dwarfs. *Astron. Astrophys.* **568,** A118 (2014).
45. Charpinet, S., Fontaine, G. & Brassard, P. Seismic evidence for the loss of stellar angular momentum before the white-dwarf stage. *Nature* **461,** 501–503 (2009).
46. Fontaine, G., Brassard, P. & Charpinet, S. The angular momentum of isolated white dwarf stars. *Astron. Soc. Pacific* **469,** 115 (2013).
47. Sullivan, D. J. Time-series spectroscopy and photometry of the helium atmosphere pulsating white dwarf EC 20058-5234. *Astron. Soc. Pac. Conf. Ser.* **509,** 315 (2017).
48. Dupret, M.-A. Nonradial nonadiabatic stellar pulsations: a numerical method and its application to a beta Cephei model. *Astron. Astrophys.* **366,** 166–173 (2001).
49. Van Grootel, V. *et al.* The instability strip of ZZ Ceti white dwarfs. I. Introduction of time-dependent convection. *Astron. Astrophys.* **539,** A87–A96 (2012).
50. Van Grootel, V., Fontaine, G., Brassard, P. & Dupret, M.-A. The newly discovered pulsating low-mass white dwarfs: an extension of the ZZ Ceti instability strip. *Astrophys. J.* **762,** 57 (2013).
51. Tremblay, P.-E. *et al.* Calibration of the mixing-length theory for convective white dwarf envelopes. *Astrophys. J.* **799,** 142 (2015).
52. Althaus, L. G. *et al.* The formation and evolution of hydrogen-deficient post-AGB white dwarfs: the emerging chemical profile and the expectations for the PG 1159-DB-DQ evolutionary connection. *Astron. Astrophys.* **435,** 631–648 (2005).
53. Kitsikis, A., Fontaine, G. & Brassard, P. Determination of a modern equation of state for the liquid/solid core of white dwarf stars. *Astron. Soc. Pac. Conf. Ser.* **334,** 65 (2005).
54. Hubbard, W.-B & Lampe, M. Thermal cnduction by electrons in stellar matter. *Astrophys. J. Suppl. Ser.* **18,** 297 (1969).
55. Cassisi, S., Potekhin, A. Y., Pietrinferni, A., Catelan, M. & Salaris, M. Updated electron-conduction opacities: the impact on low-mass stellar models. *Astrophys. J.* **661,** 1094–1104 (2007).

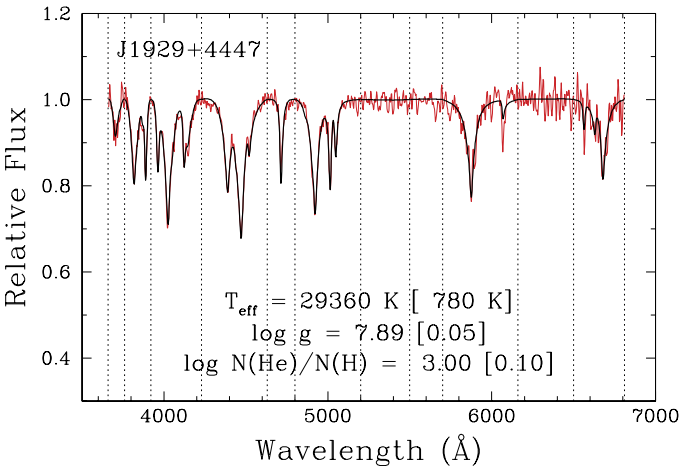

Extended Data Figure 1 | Model fit to the spectrum of KIC08626021 (catalogued as J1929+4447). The model fit is shown in black, the observed spectrum in red. Our estimates indicate that KIC08626021 is the second hottest of the known pulsators of the V777 Her type. The quoted uncertainties are only the formal errors of the fit.

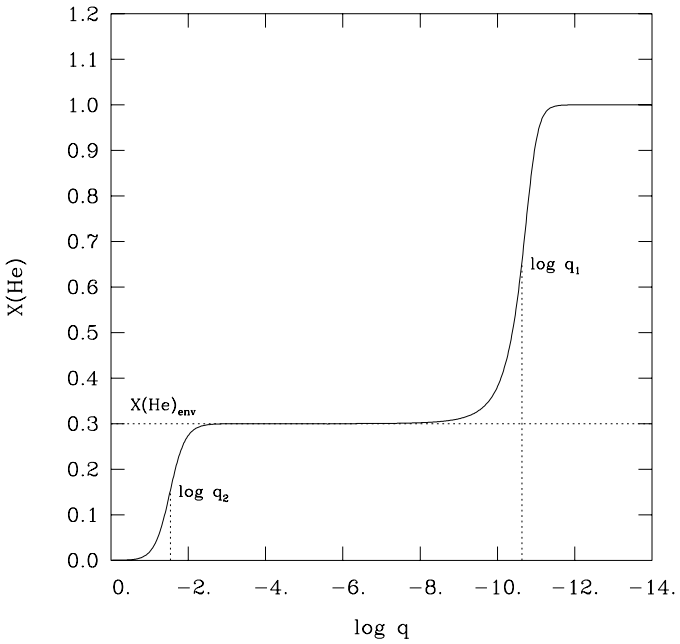

Extended Data Figure 2 | Parameterization of the helium profile in the envelope of a typical DB white dwarf model. The figure shows the local helium mass fraction, X(He), as a function of the fractional mass depth, $\log(q) \equiv \log[1-M(r)/M]$. Along with the three quantities depicted in the plot—$\log(q_1)$, $\log(q_2)$ and $X(\mathrm{He})_{\mathrm{env}}$, as defined previously—there are two other hidden parameters that are related to the shape of the helium profile in the descent centred on $\log(q_1)$ and in the descent centred on $\log(q_2)$ (see text for details).

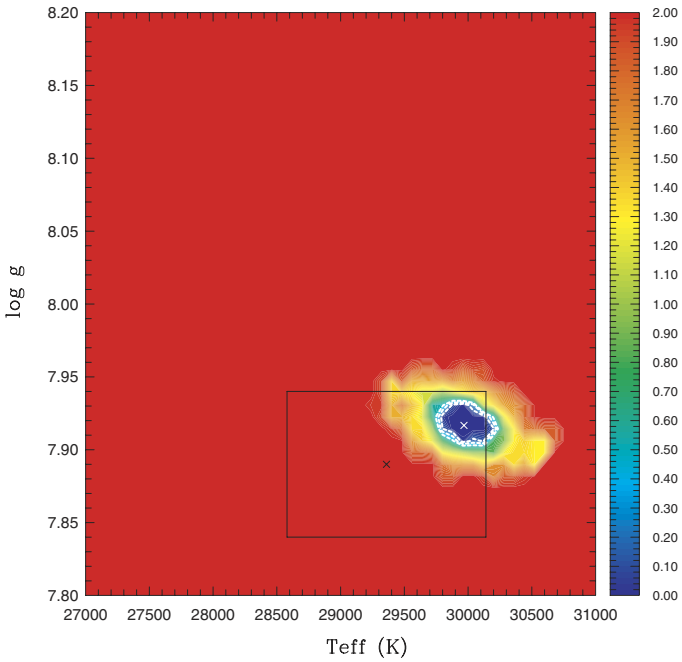

Extended Data Figure 3 | Map of the 15-dimensional merit function S^2 projected onto the log(g)–$T_{\rm eff}$ plane for models of KIC08626021. The merit function is shown on a logarithmic colour scale (base 10).The location of the optimal model in this plane is indicated by a white cross. The white dotted curves delimit the regions where the merit function has values within the 1σ, 2σ and 3σ confidence levels relative to the best-fitting solution. The black cross surrounded by the solid black box indicates the independent spectroscopic solution and its 1σ uncertainties.

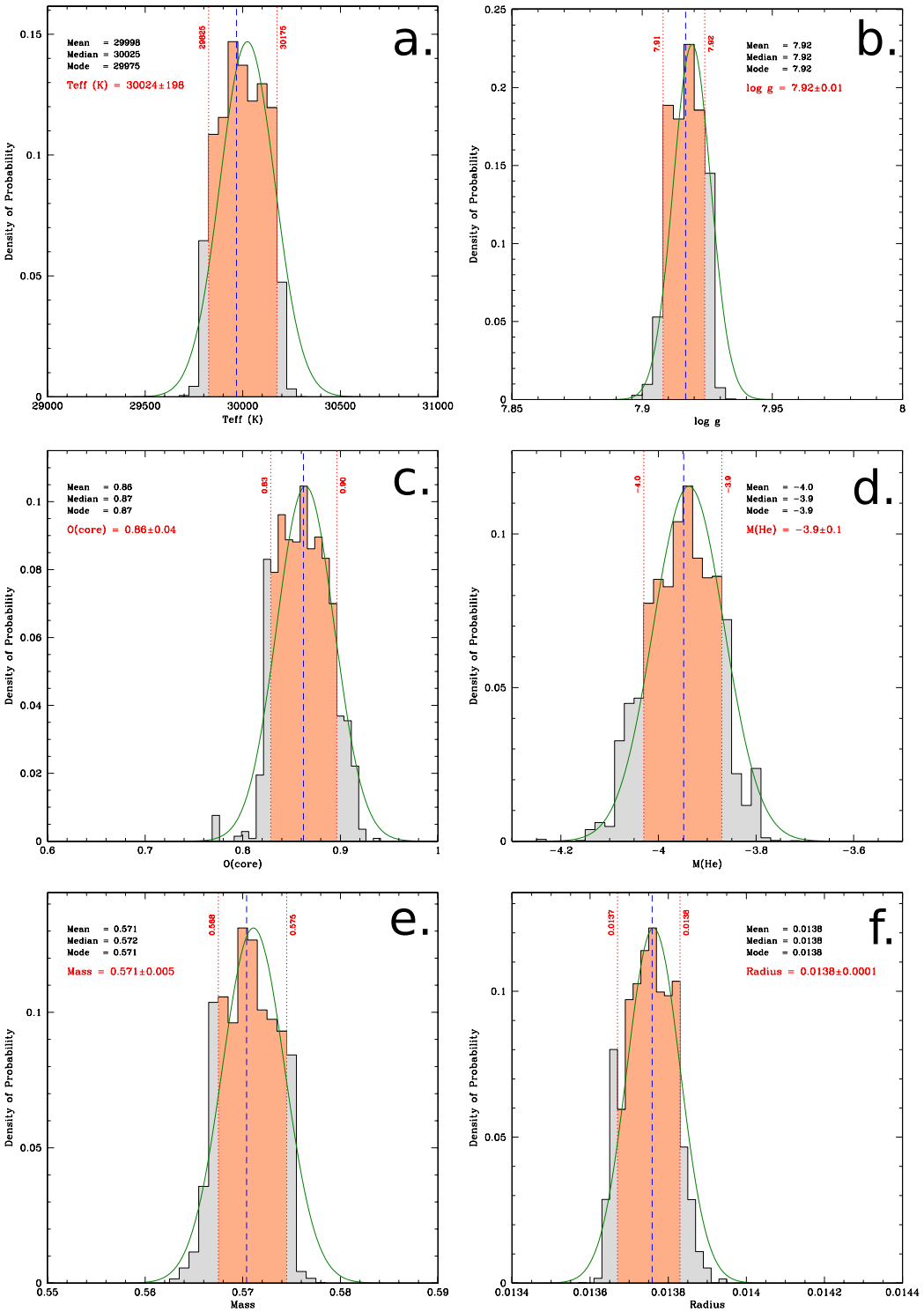

Extended Data Figure 4 | Results of the statistical analysis carried out in parameter space about the optimal seismic model for KIC08626021. Only the most interesting parameters are illustrated here. Each histogram shows the derived probability-density function for a given model parameter. The orange hatched region between the two vertical solid red lines defines the $\pm 1\sigma$ range, containing 68.3% of the distribution. The green curve defines the Gaussian fit applied to the distribution, which gives the $\pm 1\sigma$ range. The blue vertical dashed line indicates the value of the parameter of the optimal model solution. The mean, median and mode values are also indicated. The estimate of the parameter of interest, indicated in red, is the statistical value (not the optimal one) and corresponds to the central value of the $\pm 1\sigma$ interval. The various panels correspond to the following model parameters: **a**, effective temperature; **b**, surface gravity; **c**, central mass fraction of oxygen; **d**, total mass fraction of helium; **e**, total mass; and **f**, total radius of the star (in logarithmic units).

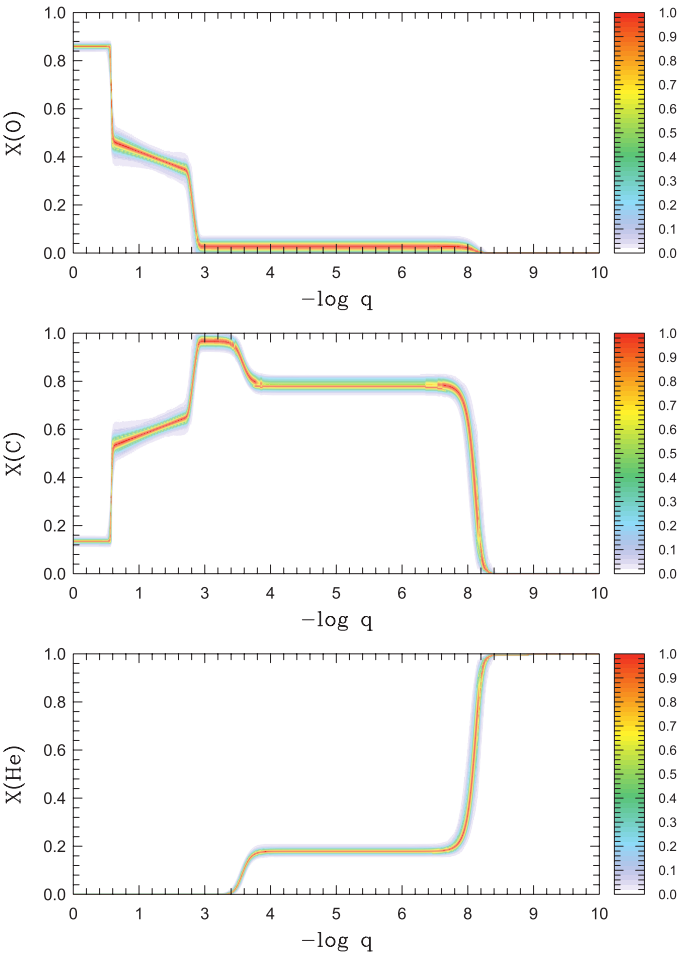

Extended Data Figure 5 | Derived probability-distribution functions, normalized to 1, for the oxygen, carbon and helium profiles.

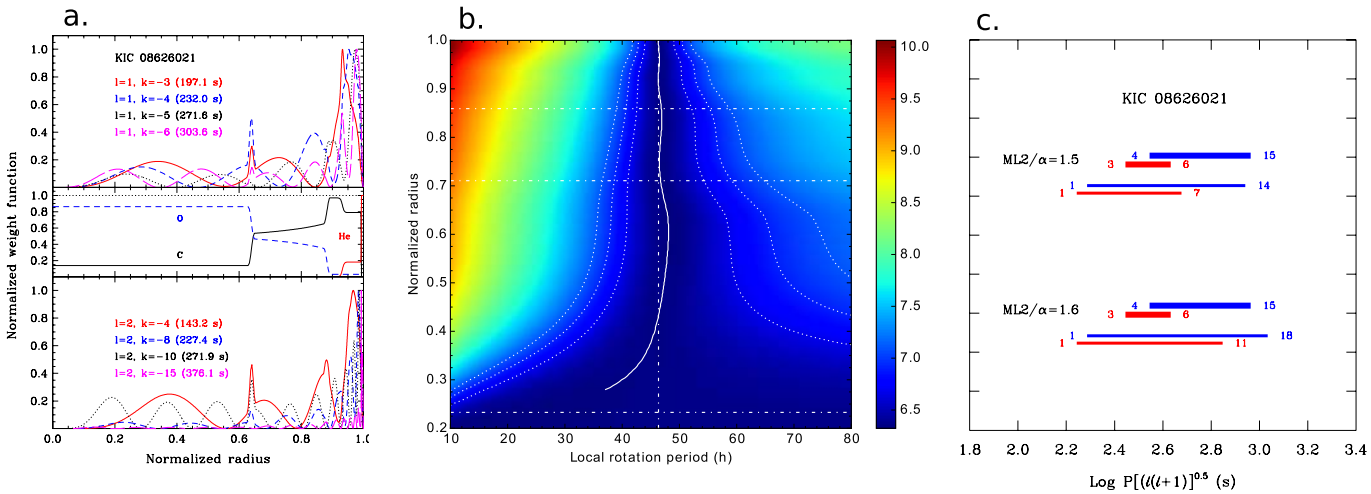

Extended Data Figure 6 | Various properties of our optimal model. **a**, Normalized weight function plotted against the normalized radius. Each individual weight function for the eight gravity modes of interest from the optimal model of KIC08626021 is normalized to a maximum value of 1.0. The weight function of a mode indicates the layers contributing most to the integral, giving the frequency (period) of the mode according to a well known variational principle in linear pulsation theory. The middle panel illustrates the chemical stratification of the model. All of the identified modes are useful probes of the core composition. **b**, Internal rotation profile. Contour map of the two-dimensional merit function that optimizes the match between the observed spacings in the three frequency multiplets with computed spacings on the basis of our seismic model. This is shown in terms of depth (expressed as the normalized radius) and in terms of the local rotation period of the inner region in the two-zone approach of ref. 45. The best-fitting solution is illustrated by the nearly vertical white curve about the solid-body solution (vertical dot-dashed white line). The dotted white curves on both sides of the solution depict its associated 1σ, 2σ and 3σ uncertainty contours. The fact that these contours diverge out at the greater depths considered here indicates that the rotationally split gravity modes available here lose their capacity to measure the local rotation rate at greater depths (indeed, their rotation kernels have negligible amplitudes at such depths). The horizontal white dot-dashed lines indicate the layer below which there is 99%, 90% and 10% of the mass of the star, from top to bottom. **c**, Comparison between the ranges of detected and excited periods in KIC08626021. The panel shows the detected periods (thick lines) with the bands of excited periods (thin lines) in two models similar to the optimal seismic model, but computed with the higher convective efficiency of ML2/$\alpha = 1.5$ (above) and ML2/$\alpha = 1.6$ (below). The reduced period is used as the abcissa in order to have comparable values for both dipole mode (in red) and quadrupole mode (in blue). The radial order k is indicated at both ends of each range.

Extended Data Table 1 | Mode identification and details of the frequency fit obtained for the optimal solution

l	k	ν_{obs} (μHz)	ν_{th} (μHz)	P_{obs} (s)	P_{th} (s)	log E (erg)	C_{kl}	ID
1	−1	...	8068.03208	...	123.945962	48.875	0.2874	
1	−2	...	6067.64155	...	164.808681	47.711	0.4012	
1	−3	5073.23411	5073.23411	197.112922	197.112922	47.181	0.4276	f_2
1	−4	4309.91490	4309.91490	232.023143	232.023143	46.678	0.4555	f_1
1	−5	3681.80286	3681.80286	271.606068	271.606068	46.197	0.4681	f_3
1	−6	3294.36928	3294.36928	303.548241	303.548241	46.018	0.4702	f_6
1	−7	...	2971.71850	...	336.505628	45.878	0.4784	
1	−8	...	2616.20375	...	382.233227	45.571	0.4834	
2	−2	...	9825.05526	...	101.780598	47.427	0.0963	
2	−3	...	8088.37817	...	123.634180	46.913	0.1098	
2	−4	6981.26129	6981.26129	143.240592	143.240592	46.557	0.1218	f_9
2	−5	...	6110.75661	...	163.645857	46.055	0.1411	
2	−6	...	5399.55096	...	185.200586	45.886	0.1440	
2	−7	...	4859.14357	...	205.797583	45.930	0.1417	
2	−8	4398.37230	4398.37230	227.356834	227.356834	45.439	0.1540	f_5
2	−9	...	3994.39516	...	250.350794	45.414	0.1528	
2	−10	3677.99373	3677.99373	271.887358	271.887358	45.365	0.1520	f_7
2	−11	...	3406.57028	...	293.550380	44.746	0.1593	
2	−12	...	3138.95972	...	318.576882	44.555	0.1575	
2	−13	...	2967.78647	...	336.951465	44.208	0.1581	
2	−14	...	2808.26351	...	356.091939	43.571	0.1622	
2	−15	2658.77740	2658.77740	376.112721	376.112721	43.540	0.1619	f_4
2	−16	...	2531.88338	...	394.962900	43.834	0.1597	

log$E$, kinetic energy of the mode (in logarithmic scale); C_{kl}, first-order solid-body rotation coefficient.

Extended Data Table 2 | Defining parameters of the optimal seismic model found for KIC08626021

Quantity	Optimum value
$T_{\rm eff}$ (K)	29,968
log g	7.9167
log q_1	−7.630
log q_2	−3.229
$X(\mathrm{He})_{\rm env}$	0.181
P_1	6.664
P_2	13.246
Core O	0.862
t1	−0.728
Δt1*	0.0294
t1(O)	0.4655
t2	−2.284
Δt2	0.132
t2(O)	0.349
$X_{\rm env}$(O)	0.0294

*A secondary parameter is defined by the relation $\log(q_3) = t_1 + \Delta t_1/2$, representing the extent in $\log(q)$ of the inner flat portion of the oxygen profile in Fig. 2. The parameter $\log(q_3)$ is used in the comparison with the results of other investigations.

Extended Data Table 3 | Observed periods, mode identification and normalized merit functions for past seismic studies of KIC08626021 compared with this work

Mode	143.24 (s)	197.11 (s)	227.36 (s)	232.02 (s)	271.61 (s)	271.89 (s)	303.55 (s)	376.11 (s)	s^2 (s^2)	References
$l, -k$	...	1,3	...	1,4	1,5	...	1,6	2,15	7.84×10^{-2}	37
$l, -k$	...	1,3	...	1,4	1,5	...	1,6	1,8	3.74	38
$l, -k$	...	1,3	...	1,4	1,5	...	1,6	1,8	2.93×10^{-2}	39*
$l, -k$	...	1,3	...	1,4	1,5	...	1,6	2,15	2.51×10^{-5}	39†
$l, -k$	2,4	1,3	2,8	1,4	1,5	...	1,6	1,8	1.31×10^{-1}	21‡
$l, -k$	2,4	1,3	2,8	1,4	1,5	...	1,6	1,8	4.80×10^{-1}	21¶
$l, -k$	2,4	1,3	2,8	1,4	1,5	2,10	1,6	2,15	1.75×10^{-16}	This work

Previous results from refs 21 and 37–39.
*Solution 1 of ref. 39.
†Solution 2 of ref. 39.
‡Solution 1 of ref. 21.
¶Solution 2 of ref. 21.

Extended Data Table 4 | Main inferred parameters from past seismic studies of KIC08626021 in comparison with this work

$\log g$ (cm s^{-2})	$T_{\rm eff}$ (K)	$M_*/M_\odot$	$\log M({\rm He})/M_*$	$\log q_1$	$\log q_2$	$\log q_3$	$X({\rm O})_{\rm center}$	References
...	29200	0.570	...	−6.30	−2.80	−0.19	0.60–0.65	37
8.099	27263	0.664	−2.27	−5.95	−1.63	−0.27	0.65	38
7.840	29990	0.539	−4.29	−7.59	−3.59	...	0.09	39*
7.900	28750	0.563	−1.91	−6.22	−0.91	...	0.89	39†
...	29650	0.550	...	−7.90	−3.10	−0.11	0.55	21‡
...	29350	0.550	...	−8.40	−3.00	−0.11	0.70	21¶
7.917(9)	29968(150)	0.570(4)	−3.95(3)	−7.63(9)	−3.23(5)	−0.72(1)	0.86(2)	This work

Previous results from refs 21 and 37–39.
*Solution 1 of ref. 39.
†Solution 2 of ref. 39.
‡Solution 1 of ref. 21.
¶Solution 2 ofref. 21.